Inhibition and Binding Kinetics of the Hepatitis C Virus NS3 Protease Inhibitor ITMN-191 Reveals Tight Binding and Slow Dissociative Behavior

Ravi Rajagopalan,*,‡ Shawn Misialek,‡ Sarah K. Stevens,‡ David G. Myszka,§ Barbara J. Brandhuber,|| Joshua A. Ballard,|| Steven W. Andrews,|| Scott D. Seiwert,‡ and Karl Kossen‡

InterMune Inc., 3280 Bayshore Boulevard, Brisbane, California 94005, Biosensor Tools, 1588 East Connecticut Drive, Salt Lake City, Utah 84132, and Array Biopharma, 3200 Walnut Street, Boulder, Colorado 80301

Received January 9, 2009; Revised Manuscript Received February 9, 2009

ABSTRACT: The protease activity of hepatitis C virus nonstructural protein 3 (NS3) is essential for viral replication. ITMN-191, a macrocyclic inhibitor of the NS3 protease active site, promotes rapid, multilog viral load reductions in chronic HCV patients. Here, ITMN-191 is shown to be a potent inhibitor of NS3 with a two-step binding mechanism. Progress curves are consistent with the formation of an initial collision complex (EI) that isomerizes to a highly stable complex (EI*) from which ITMN-191 dissociates very slowly. K_i, the dissociation constant of EI, is 100 nM, and the rate constant for conversion of EI to EI* is 6.2×10^{-2} s^{-1}. Binding experiments using protein fluorescence confirm this isomerization rate. From progress curve analysis, the rate constant for dissociation of ITMN-191 from the EI* complex is 3.8×10^{-5} s^{-1} with a calculated complex half-life of ~5 h and a true biochemical potency (K_i*) of ~62 pM. Surface plasmon resonance studies and assessment of enzyme reactivation following dilution of the EI* complex confirm slow dissociation and suggest that the half-life may be considerably longer. Abrogation of the tight binding and slow dissociative properties of ITMN-191 is observed with proteases that carry the R155K or D168A substitution, each of which is likely in drug resistant mutants. Slow dissociation is not observed with closely related macrocyclic inhibitors of NS3, suggesting that members of this class may display distinct binding kinetics.

Approximately 170 million people worldwide are chronically infected with the hepatitis C virus (HCV),[1] which if untreated causes liver fibrosis and cirrhosis (*1*). HCV is also the leading cause of liver transplantations in the United States (*2*). The current standard of care (SOC) combination therapy of pegylated interferon-α and ribavirin has undesirable side effects and achieves a sustained virologic response (SVR) in only ~50% of genotype 1 patients (the dominant genotype in the United States) (*3, 4*). Currently, new drugs targeting HCV-encoded enzymes are being evaluated in clinical trials and have shown viral load reductions when administered both as monotherapies and in combination with SOC (*5, 6*). Of the virus-encoded enzymes, the majority of drug candidates target either the protease activity of nonstructural (NS) protein NS3 or viral polymerase NS5B.

* To whom correspondence should be addressed. Telephone: (415) 466-2277. Fax: (415) 466-2377. E-mail: rrajagopalan@intermune.com.
‡ InterMune Inc.
§ Biosensor Tools.
|| Array Biopharma.

[1] Abbreviations: HCV, hepatitis C virus; SOC, standard of care; SVR, sustained virologic response; NS3, NS4A, NS4B, NS5A, and NS5B, nonstructural proteins 3, 4A, 4B, 5A, and 5B, respectively; HEPES, 4-(2-hydroxyethyl)-1-piperazineethanesulfonic acid; Tris-HCl, tris(hydroxymethyl)aminomethane hydrochloride; DTT, dithiothreitol; PCR, polymerase chain reaction; IPTG, isopropyl β-D-thiogalactopyranoside; CHAPS, 3-[(3-cholamidopropyl)dimethylammonio]-1-propane sulfonate; LDAO, lauryldimethylamine *N*-oxide; sulfo-NHS-LC-LC-biotin, sulfosuccinimidyl-6′-(biotinamido)-6-hexanamido hexanoate; DMSO, dimethyl sulfoxide; WT NS3, wild-type NS3; HIV-1, human immunodeficiency virus strain 1; MDR, multidrug resistant.

NS3 is a bifunctional protein containing both protease and helicase domains. The 187 N-terminal residues of the NS3 protein encode a chymotrypsin-like serine protease that requires viral protein cofactor NS4A. NS4A stabilizes the protein fold to properly form the catalytically competent protease active site (*7*−*9*). Previous studies have shown that a minimal 14-amino acid peptide can substitute for NS4A to achieve high levels of activity in biochemical assays (*10*−*12*). The activated NS3 protease cleaves the viral polypeptide at four sites to liberate the functional forms of NS3, NS4A, NS4B, NS5A, and NS5B proteins that are required for viral replication. The NS3 protease has also been shown to suppress the innate immune response by cleavage of host proteins (*13*−*16*).

BILN-2061 was the first NS3 protease inhibitor to demonstrate viral load reductions in HCV-infected patients (*17*). BILN-2061 (ciluprevir) is highly potent against HCV genotype 1 in both biochemical and HCV replicon assays. However, clinical development of BILN-2061 was halted following observation of cardiac toxicity in rhesus monkeys (*18*). A separate class of linear tetrapeptide inhibitors contains a ketoamide functionality that is designed to form a covalent adduct with NS3. This class includes VX-950 (telaprevir) and SCH-503034 (boceprevir) which are currently in late stage clinical trials (*5, 6*). These ketoamide-based inhibitors bind to NS3 in a two-step mechanism to reversibly form a covalent enzyme inhibitor complex from which they dissociate slowly (*19*−*21*). Other NS3 protease inhibitors currently being evaluated in clinical trials include the macro-

10.1021/bi900038p CCC: $40.75
Published on Web 02/11/2009

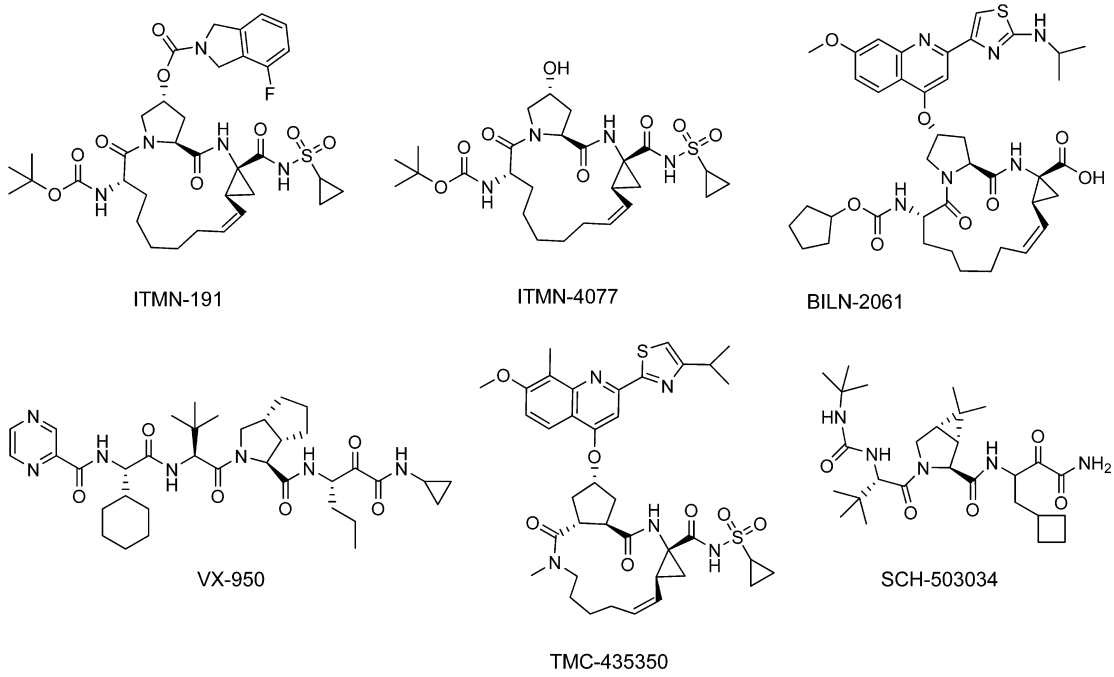

FIGURE 1: Chemical structures of HCV NS3 protease inhibitors.

cyclic inhibitors TMC-435350 and ITMN-191 (Figure 1) (*5, 6*). In phase 1b clinical trials, treatment for 14 days with 200 mg of ITMN-191 on twice and thrice daily schedules yielded mean maximum HCV RNA $\log_{10}$ reductions of 3.4 and 3.9, respectively (*22*−*24*). The preclinical characteristics of ITMN-191 summarized elsewhere include (*25*) (i) high in vitro selectivity against a broad panel of proteases, other enzymes, and receptors; (ii) highly potent activity in the cell-based HCV replicon assay; (iii) synergy with pegylated interferon-α-2a; and (iv) preferential distribution to liver.

Here, we present a kinetic characterization of NS3 protease inhibition by ITMN-191. A two-step tight binding mechanism is proposed, and estimates for the individual rate constants are provided. The data support the formation of a highly stable, noncovalent enzyme inhibitor complex from which ITMN-191 dissociates extremely slowly.

MATERIALS AND METHODS

Materials. ITMN-191, [^{14}C]ITMN-191, ITMN-4077, VX-950, and BILN-2061 were synthesized by InterMune or a commissioned contractor. The NS4A peptide cofactor was obtained from Midwest Biotech (Fishers, IN). The FRET-based assay substrate [sequence, Ac-DE-Dap(QXL520)-EE-AbuΨ[COO]-AS-Cys(5-FAMsp)-NH_2] was obtained from Anaspec, Inc. (San Jose, CA). Enzyme assay and protein fluorescence data were collected on a SpectraMax M5 plate reader (Molecular Devices, Sunnyvale, CA) using plate or cuvette read modes. Excitation, emission, and cutoff filter wavelengths for enzyme assays were set to 490, 520, and 515 nm, respectively. For protein fluorescence, these were set to 280, 340, and 325 nm, respectively.

NS3 Proteins. Sequences for HCV NS3 and NS4A (Supporting Information) were derived from a plasmid encoding the genotype 1b-K2040 replicon which was kindly provided by M. Gale (University of Washington, Seattle, WA) (*26*). The N-terminally $(His)_6$-tagged full-length 1b-K2040 NS3 protein was obtained as follows. The K2040 NS3 gene was cloned into a variant of the pVL1392 transfer vector (BD Biosciences, San Jose, CA). Recombinant baculoviruses were then created using the Baculogold System (BD Biosciences). A P3 viral stock was generated and used to infect 1 L of High Five insect cells at an initial multiplicity of infection (MOI) of 0.5. Forty-eight hours postinfection, cells were pelleted via centrifugation, lysed via mild sonication, and His_6-tagged NS3 purified by Ni affinity immobilization. The eluted protein was further purified by gradient chromatography on poly(U) Sepharose followed by gel filtration chromatography (Superdex 200). During purification, the protein concentration was maintained at ∼1 mg/mL by ultrafiltration with Amicon YM10 filters. Purified NS3 at ∼1 mg/mL in storage buffer [25 mM HEPES (pH 7.5), 300 mM potassium chloride, 0.1% β-octyl glucoside, 10 mM DTT, and 10% glycerol] was frozen in small aliquots for long-term storage. D168A and R155K variants of NS3 were introduced into the pVL1392 transfer vector and used to produce mutant proteins in the full-length K2040 NS3 background using the methods described above.

Isolation of the NS3•NS4A heterodimer protein complex was based on a previously published method (*27*). Briefly, the coding sequence for the 54 residues of NS4A and the 16 N-terminal residues of NS4B were cloned into the C-terminal end of the NS3 coding sequence in the pVL1392-NS3 construct (see above). This allows for the expression of an N-terminally His_6-tagged viral polypeptide that autoprocesses to yield the NS3•NS4A noncovalent heterodimer complex (*27*). The pVL1392-based transfer vector generated was used to express the viral polypeptide in High Five insect cells. Cell lysis, extraction, and purification via Ni-NTA immobilization and gel filtration chromatography (Superdex 200) were performed as described previously (*27*). Purified NS3•NS4A at ∼1 mg/mL in storage buffer [50 mM sodium phosphate (pH 8.0), 300 mM sodium chloride, 0.05% dodecyl β-D-maltoside, 10 mM DTT, and 10% glycerol] was

frozen in small aliquots for long-term storage. N-Terminal sequencing confirmed the presence of NS4A in the purified protein.

The NS3Δ (protease domain of NS3) enzyme of genotype 1b-K2040 was obtained as follows. A PCR fragment encoding the initial 188 residues of NS3 was obtained by amplification from the pVL1392-NS3 construct (see above) and cloned into a pET-based vector (Novagen, Madison, WI) for the expression of NS3Δ without any affinity tags. Transformed BL21(DE3) cells were grown at 37 °C to an OD_{600} of approximately 2 and cooled to 16 °C prior to induction with 1 mM IPTG and overnight expression at a reduced temperature. The harvested cells were lysed, and the clarified supernatant was purified by SP-Sepharose chromatography using a linear sodium chloride gradient. The NS3Δ-containing fractions were pooled and dialyzed prior to heparin Sepharose purification with a linear salt gradient. The purified eluate was then concentrated and further purified by size exclusion chromatography (HiLoad Superdex 200). The purified NS3Δ at ~6 mg/mL in storage buffer [25 mM HEPES (pH 7.5), 150 mM sodium chloride, 0.1% CHAPS, 5 mM DTT, and 10% glycerol] was frozen in small aliquots for long-term storage.

All proteins used in this study were expressed and purified for InterMune by Proteos Inc. (Kalamazoo, MI).

Enzyme Assays. All NS3 assays were conducted at ambient temperature (23 °C) in assay buffer containing 50 mM Tris-HCl (pH 7.5), 15% glycerol, 0.6 mM LDAO, 25 μM NS4A peptide, and 10 mM DTT. This was prepared prior to use by addition of NS4A peptide and DTT to a mixture of the other components that is stored at 4 °C. Working stock solutions of enzyme and substrate were also prepared immediately prior to use by dilution with assay buffer. The FRET-based peptide substrate was used at 0.5 μM in all ITMN-191 inhibition assays.

For k_{cat} and K_m determinations, the substrate concentration was varied from 0.1 to 10 μM. Reactions were initiated in a 96-well plate by the addition of 50 pM NS3 enzyme. Initial rates calculated over the first 30 min of the reaction were plotted against substrate concentration and fit to the Michaelis−Menten equation to yield K_m and V_{max} values (KaleidaGraph, Synergy Software Inc., Reading, PA). k_{cat} values were calculated from V_{max} using the extinction coefficient of product peptide and enzyme concentrations determined from active site titrations. k_{cat} and K_m are reported as means ± the standard deviation (SD) of three data sets.

Progress Curves of NS3 Inhibition by ITMN-191. Reaction mixtures containing specified concentrations of NS3 (50 pM to 5 nM) and ITMN-191 (78 pM to 1000 nM) were set up in 96-well plates or cuvettes as follows. Reactions were initiated by addition of NS3 to assay buffer containing 0.5 μM substrate and ITMN-191. Typically, separate 20× working stocks of substrate, ITMN-191, and NS3 were prepared and used to assemble 200 μL reaction mixtures by adding 10 μL of each (in that order) to 170 μL of assay buffer. Control reactions (i) without ITMN-191 and (ii) without NS3 were performed simultaneously. Progress curve data were collected for up to 5 h and analyzed.

Dilution of NS3·ITMN-191 Complexes. Complexes of NS3 enzymes with ITMN-191 were formed by incubating 1 μM NS3 with 2 μM ITMN-191 for 15 min in assay buffer. At 2 μM ITMN-191, the WT and mutant NS3s studied here are fully inhibited. These preformed complexes were used to initiate reactions by a rapid 10000-fold dilution to final NS3 and ITMN-191 concentrations of 0.1 and 0.2 nM, respectively. The 10000-fold dilution was typically obtained by two sequential 100-fold dilutions into assay buffer containing substrate. Typical assay reaction volumes were 200 μL with progress curve data collection for up to 4 h. The following control reactions were run alongside the others: (i) a negative control lacking NS3 to account for the background substrate hydrolysis rate, (ii) a maximal rate control with the same final concentration of NS3 (no ITMN-191), and (iii) a control reaction lacking exposure of NS3 to ITMN-191 prior to reaction that has the same final NS3 and ITMN-191 concentrations attained by dilution of the preformed complexes. The final control was initiated by adding NS3 to the assay well containing substrate and ITMN-191.

NS3 Protein Fluorescence. The intrinsic fluorescence of protease domain enzyme NS3Δ has previously been used to study the kinetics of inhibitor binding (*21*). Under these experimental conditions, a minimum of 0.3 μM NS3Δ was required to obtain appropriate levels of fluorescence. Typically, 10 μL of a concentrated ITMN-191 solution in assay buffer was added to 0.3 μM NS3Δ in 3 mL of assay buffer in a quartz cuvette. Data were collected immediately following ITMN-191 addition.

Surface Plasmon Resonance Experiments. Experiments were conducted on a Biacore T100 instrument with data analysis using Scrubber2 (Biologica Software Pty Ltd.). Minimal biotinylation of the purified NS3·NS4A complex was achieved by reaction with sulfo-NHS-LC-LC-biotin (Pierce Biotech) on ice for 1 h followed by desalting into running buffer [50 mM Tris-HCl (pH 7.5), 15% glycerol, 1 mM DTT, and 3% DMSO]. The biotinylated NS3·NS4A complex was then immobilized to a streptavidin-coated sensor surface. For dissociation rate experiments, 1 μM ITMN-191, 1 μM BILN-2061, 3 μM VX-950, and 3 μM ITMN-4077 were tested with the prepared surface. Due to very slow dissociation rates, a newly prepared protein-coated surface was used for each experiment. Binding rate constants were extracted from sensorgram data by fitting to a 1:1 interaction model.

Dissociation of Radiolabeled ITMN-191. All reagents were prepared in assay buffer. A limiting amount of [^{14}C]ITMN-191 (2 μM) was bound stoichiometrically via addition of a slight excess of WT NS3 (3 μM) and incubation for 15 min. Competition was initiated by the addition of 1 mM unlabeled ITMN-191 to a reaction volume of 1 mL. At designated time points, 100 μL aliquots were withdrawn and centrifuged at 14000*g* through YM-50 Microcon columns (Millipore, Billerica, MA). The radioactivity in the filtrate was measured by liquid scintillation counting and reflects the amount of unbound [^{14}C]ITMN-191. Control reactions (i) without NS3 and (ii) with excess unlabeled ITMN-191 added to NS3 prior to [^{14}C]ITMN-191 produced the expected total release of counts into the filtrate.

Simulation of ITMN-191 Binding Kinetics. Progress curves from enzyme-initiated reactions were used to globally simulate binding kinetics using KinTek Global Kinetic Explorer (KinTek Corp., Austin, TX). The two-step inhibition model was defined in the software, and data were globally fit while the substrate concentration, k_{cat}, and K_m values were

Table 1: Steady-State Kinetic Parameters for NS3 Protease and Its Derivatives[a]

enzyme	K_m (μM)	k_{cat} (s^{-1})	k_{cat}/K_m (μM^{-1} s^{-1})
WT NS3	0.6 ± 0.1	0.18 ± 0.02	0.30 ± 0.06
D168A NS3	0.6 ± 0.1	0.27 ± 0.02	0.45 ± 0.08
R155K NS3	0.22 ± 0.04	0.25 ± 0.02	1.1 ± 0.2
WT NS3Δ	0.34 ± 0.03	0.11 ± 0.01	0.32 ± 0.04

[a] Values are expressed as means ± SD of three independent data sets.

applied and the inhibition rate and equilibrium constants were appropriately constrained.

RESULTS

Catalytic Properties of NS3 Proteins. Catalytic constants k_{cat} and K_m for cleavage of the fluorescence-quenched peptide substrate were measured for the various genotype 1b NS3 proteases used in this study (Table 1). Deletion of the C-terminal helicase domain from NS3 (NS3Δ) has a minimal effect on protease activity as noted previously (*28*). In replicon-based drug resistance studies, R155K and D168A mutations result in a significant loss of ITMN-191 potency (*29, 30*). These mutations do not reduce catalytic efficiency on the substrate employed (Table 1).

Progress Curve Analysis of NS3 Inhibition by ITMN-191. Progress curves of reactions initiated by addition of NS3 show clear biphasic character and are consistent with a slow onset of ITMN-191 inhibition. Representative progress curves collected at lower (Figure 2A) and higher (Figure 2B) ITMN-191 concentrations are shown separately to account for the different reaction time scales and protein concentrations used in the assays. Traces for control reactions without ITMN-191 are linear over the time frame during which biphasic character is observed. Identical progress curve data were obtained for NS3Δ, indicating no difference in ITMN-191 inhibition between full-length and protease domain enzymes (data not shown). While progress curves obtained with ITMN-191 and WT NS3 are clearly biphasic and consistent with time-dependent inhibition, experiments with D168A and R155K NS3 enzymes gave quasi-linear traces in the presence of ITMN-191, indicating that the slow binding property may be compromised by these mutations (Supporting Information).

Two common mechanisms have been described for slow binding inhibitors (Scheme 1). The first example is a simple one-step mechanism in which inherently low values for association and dissociation rate constants (k_1 and k_2) give rise to the observation of slow binding (Scheme 1A). Examples include the inhibition of angiotensin converting enzyme (ACE) by captopril and enalapril (*31*) and the inhibition of factor Xa by PD0313052 (*32*). Alternatively, a two-step mechanism is possible, where an initial complex (EI) is formed and then slowly converts to a more stable state (EI*) (Scheme 1B). Examples include the inhibition of HIV-1 protease by peptidomimetic drugs (*33, 34*) and the inhibition of HCV NS3 protease by ketoamide inhibitors, such as VX-950 (*19*−*21*).

These two mechanisms can be differentiated on the basis of an analysis of progress curves obtained in the presence of increasing inhibitor concentrations and the kinetics of protein inactivation. In both mechanisms, the steady-state rate for enzyme-initiated reactions is predicted to be dependent on inhibitor concentration. However, the two mechanisms differ with respect to the inhibitor dependence of the initial rate. The initial rates of the one- and two-step binding mechanisms are predicted to be independent and dependent on ITMN-191 concentration, respectively (*35*). Both initial and steady-state rates are dependent on ITMN-191 concentration (Figure 2), thereby supporting a two-step inhibition mechanism like that shown in Scheme 1B.

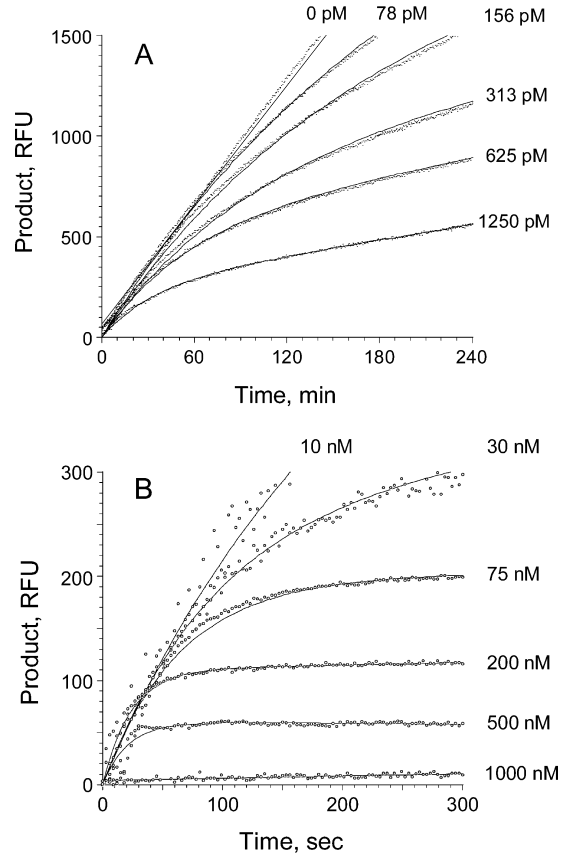

FIGURE 2: Reaction progress curves for the inhibition of WT NS3 by ITMN-191. All reactions were initiated by NS3 addition. (A) Inhibition of 50 pM WT NS3 by 0, 78, 156, 313, 625, and 1250 pM ITMN-191. (B) Inhibition of 0.5 nM WT NS3 by 10, 30, and 75 nM ITMN-191 and inhibition of 5 nM WT NS3 by 200, 500, and 1000 nM ITMN-191. Solid lines represent curve fitting using eq 1 to extract k_{obs} for inactivation.

Scheme 1: Inhibition Mechanisms Involving (A) One-Step and (B) Two-Step Binding Modes

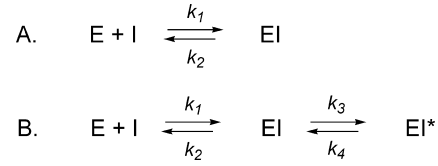

The mechanisms in Scheme 1 can be further differentiated on the basis of the inhibitor dependence of k_{obs}, a first-order rate constant for ITMN-191-dependent inactivation of NS3. The value of k_{obs} at each inhibitor concentration was obtained by fitting the progress curves in Figure 2 to eq 1 which relates product fluorescence at time t and time zero (F_t and F_0, respectively) to k_{obs} and the initial (V_0) and steady-state (V_s) reaction rates (*35*).

$$F_t = F_0 + V_s t + (V_0 - V_s)[1 - \exp(-k_{obs} t)]/k_{obs} \quad (1)$$

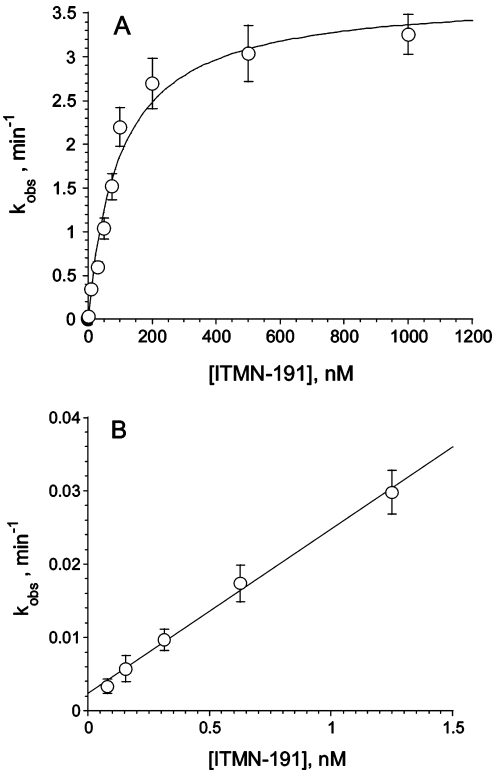

FIGURE 3: Dependence of WT NS3 inactivation rate (k_{obs}) on ITMN-191 concentration. (A) k_{obs} from the analysis of data in Figure 2 is plotted and fit to eq 2. The fitted maximal rate and inhibition constants (K_i) are 0.062 ± 0.003 s^{-1} and 100 ± 10 nM, respectively. (B) Plot of k_{obs} at low ITMN-191 concentrations fit to the linear form of eq 2. The y intercept provides an estimate of k_4 equal to 0.0023 ± 0.0006 min^{-1} (3.8×10^{-5} s^{-1}).

The progress curves in Figure 2 are readily fit to eq 1. The k_{obs} values obtained are plotted as a function of ITMN-191 concentration (Figure 3A). The proposed one- and two-step binding mechanisms are predicted to show linear and hyperbolic dependence of k_{obs} on inhibitor concentration, respectively. The hyperbolic dependence observed thus supports a two-step binding mechanism (Figure 3A).

Microscopic rate constants in the two-step binding mechanism of ITMN-191 can be obtained from a fit of k_{obs} versus inhibitor concentration data to eq 2 (*35*).

$$k_{obs} = k_4 + k_3[I]/(K_i + [I]) \quad (2)$$

The maximal inactivation rate obtained from the fit is 6.2×10^{-2} s^{-1} and equals $k_4 + k_3$. Since the y intercept (i.e., k_4) is negligibly small, $k_4 + k_3 \simeq k_3 = 6.2 \times 10^{-2}$ s^{-1}. The concentration of ITMN-191 required to reach half-maximal rate represents the dissociation constant (K_i) of the initial complex (EI), and $K_i = k_2/k_1$. This K_i value was determined to be 100 nM.

An upper limit of the dissociation rate constant can be determined from the inhibitor dependence of k_{obs} at low concentrations of ITMN-191. Under these conditions, where K_i is significantly greater than the inhibitor concentration, eq 2 reduces to the linear form $k_{obs} = k_4 + (k_3/K_i)[I]$. The y intercept (k_4) provides an estimate of the rate of conversion of EI* to EI. Fitting k_{obs} data at low ITMN-191 concentrations to the linear equation above gives an intercept (k_4) value of 3.8×10^{-5} s^{-1} (Figure 3B). The low k_4 value suggests a very slow conversion of EI* to EI and provides an upper limit for the dissociation of ITMN-191 from NS3. Assuming that k_4 is the rate-limiting step for ITMN-191 dissociation, the half-life of the EI* complex is calculated to be ~5 h. The true biochemical potency (K_i*) of ITMN-191 can be calculated from eq 3 below to be ~62 pM (*35*). Experiments to directly measure k_4 are presented below.

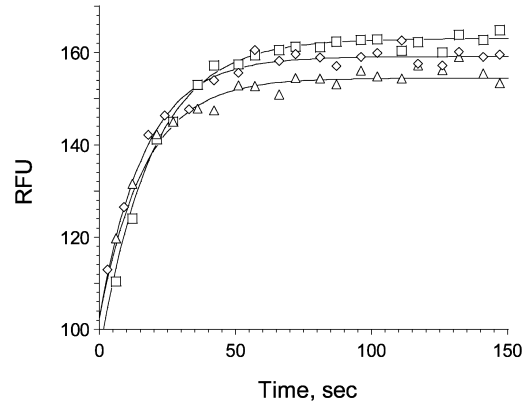

FIGURE 4: Effect of ITMN-191 binding on NS3Δ fluorescence. The increase in 0.3 μM NS3Δ fluorescence upon addition of 1 (△), 10 (◇), and 100 μM ITMN-191 (□) is shown. The kinetic traces were fit to the single-exponential function $F = F_0 + C[1 - \exp(-kt)]$, where the fluorescence (F) increase from an initial value F_0 to a maximal value of $F_0 + C$ is used to extract the first-order rate constant (k). The rate constant is invariant in the ITMN-191 concentration range tested and is 0.058 ± 0.004 s^{-1}.

$$K_i^* = k_4K_i/(k_3 + k_4) \quad (3)$$

Binding of ITMN-191 Monitored by Protein Fluorescence. Intrinsic NS3Δ protein fluorescence has previously been used to study the binding kinetics of ketoamide inhibitors (*21*). With these inhibitors, the observed NS3Δ fluorescence increase was primarily associated with the formation of EI* from EI. Here, NS3Δ fluorescence was found to similarly increase upon addition of ITMN-191. Kinetic traces for NS3Δ fluorescence at multiple ITMN-191 concentrations are presented in Figure 4. These data are described well by single-exponential fits from which a first-order rate constant can be obtained. Limited experimental sensitivity necessitates the use of a high NS3Δ concentration which in turn limits data collection to high ITMN-191 concentrations. At ITMN-191 concentrations of ≥ 1 μM, the observed rate of 5.8×10^{-2} s^{-1} is independent of inhibitor concentration and represents the rate constant k_3 for the conversion of EI to EI* in the proposed two-step mechanism. This value is in good agreement with the value of 6.2×10^{-2} s^{-1} derived from progress curve analysis.

For the full-length NS3 enzyme, there is a large fluorescence contribution from the additional helicase domain that is insensitive to the binding of protease inhibitors. Although this lowered the dynamic range of measurement significantly, a similar transition and rate was observed (data not shown).

Surface Plasmon Resonance Studies of ITMN-191 Binding. Surface plasmon resonance studies were used to directly assess the rate of ITMN-191 dissociation. Initial attempts to use NS3 with a synthetic NS4A peptide (as in the experiments described above) were unsuccessful due to the nonspecific binding of the NS4A peptide to the sensor surface. Use of a heterodimeric NS3·NS4A protein complex in which expression of an NS3−4A−4B fusion leads to

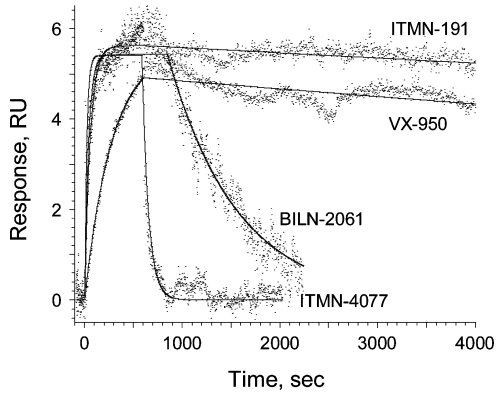

FIGURE 5: Dissociation of NS3 protease inhibitors observed by surface plasmon resonance. Sensorgram data for dissociation of ITMN-191, VX-950, BILN-2061, and ITMN-4077 from the immobilized NS3·NS4A complex were collected and analyzed as described in Materials and Methods. The dissociation rate constants for ITMN-191, VX-950, BILN-2061, and ITMN-4077 are estimated to be $<2.1 \times 10^{-5}$, $<3.7 \times 10^{-5}$, 1.4×10^{-3}, and $>1.5 \times 10^{-2}$ s^{-1}, respectively.

autoprocessing and the production of a stable NS3−4A complex eliminates the need for addition of exogenous 4A peptide (*27*). Sensorgrams were obtained for dissociation of ITMN-191, ITMN-4077, VX-950, and BILN-2061 from a minimally biotinylated NS3·NS4A complex immobilized to a streptavidin-coated sensor surface (Figure 5). ITMN-4077 is a less potent macrocyclic inhibitor that lacks the P2 isofluoroindoline group and carbamate linker of ITMN-191.

Dissociation of ITMN-4077 is rapid ($>1.5 \times 10^{-2}$ s^{-1} with an estimated enzyme inhibitor complex half-life of <46 s), indicating that the P2 element is important for slow dissociative behavior. Under similar conditions, the BILN-2061 dissociation rate constant is $\sim 1.4 \times 10^{-3}$ s^{-1} (half-life of ~8 min), which is slower than previously reported but consistent with rapid dissociation (*17*). Both VX-950 and ITMN-191 exhibit very little dissociation on the time scale of the experiment. Consequently, their dissociation rate constants can only be approximated as being lower than 3.7×10^{-5} s^{-1} ($t_{1/2} > 5$ h) and 2.1×10^{-5} s^{-1} ($t_{1/2} > 9$ h), respectively. The half-life of the NS3·VX-950 complex has been previously reported to be ~1 h (*19*). A comparison of results is complicated by protein sequence and assay differences between the two studies, but it is notable that both studies suggest slow dissociation of VX-950. The data presented here provide direct evidence of a very slow dissociation of ITMN-191 from NS3.

Dilution of NS3·ITMN-191 Complexes. Monitoring enzyme reactivation following rapid dilution of an enzyme−inhibitor complex is used to test the reversibility of inhibition and obtain estimates of dissociation rates (*35, 36*). Reactivation of WT and mutant NS3 enzymes following dilution of their respective ITMN-191 complexes was examined (Figure 6). The WT and mutant NS3 complexes were formed by incubating 1 μM NS3 with 2 μM ITMN-191. At this ITMN-191 concentration, all the NS3 enzymes studied are fully inhibited. Data collection was initiated upon dilution of these preformed complexes into buffered substrate.

Upon dilution of the WT NS3·ITMN-191 complex, negligible reactivation was observed over 2 h (Figure 6A). In contrast, the same dilution completely reactivated R155K NS3 (Figure 6C). A close inspection of the R155K NS3 curve shows a lag phase consistent with a measurable dissociation rate (Figure 6D). The curve is well-defined by eq 1, and the observed rate of reactivation is 9×10^{-3} s^{-1}. Assuming that ITMN-191 dissociation is rate-limiting in reactivation, the R155K NS3·ITMN-191 complex half-life is ~77 s. Dilution of the D168A NS3·ITMN-191 complex produces an immediate and complete reactivation that is too fast for accurate measurement of a rate (data not shown).

For WT NS3, the progress curve following complex dilution indicates minimal reactivation relative to the background reaction without enzyme (Figure 6A). On a reduced *y*-axis scale (Figure 6B), the progress curve is largely linear with a very small amount of activity being recovered at the end of the 2 h experiment. Consequently, a reliable measure of the steady-state rate (V_s) and a fit to eq 1 could not be achieved. Instead, an iterative analysis similar to the study of dissociation of actinonin from peptide deformylase was used (*36*). The conversion of EI* to EI was assumed to be rate-limiting to enzyme reactivation; i.e., $k_4 \approx k_{obs}$ in eq 1. An initial K_i* estimate of 62 pM calculated from progress curve analysis of NS3-initiated reactions was used to calculate V_s with eq 4.

$$V_{max}/V_s = 1 + (K_m/[S])(1 + [I]/K_i^*) \quad (4)$$

The rate V_{max} was taken from an uninhibited reaction, and [S], [I], and K_m were 0.5 μM, 0.2 nM, and 0.6 μM, respectively. The calculated V_s and the k_4 of 3.8×10^{-5} s^{-1} ($t_{1/2} = 5$ h) were used to generate a simulated progress curve (identified in Figure 6B by $t_{1/2}$). In an attempt to better fit the experimental trace, k_4 was reduced 3-fold ($t_{1/2} = 15$ h) in the second iteration. Using eq 3, K_i* was recalculated on the basis of the new k_4, thereby enabling the calculation of a new V_s and the generation of a new curve. k_4 was incrementally lowered to 1.3×10^{-6} s^{-1} ($t_{1/2} = 6$ days) until a satisfactory overlap of the modeled data and experimental trace was achieved (Figure 6B). Using this k_4 value, K_i* was calculated to be 2.2 pM.

For very slowly dissociating inhibitors, incubation for extended times could potentially increase the percentage of reactivated enzyme and improve the dissociation rate estimation. Very slow dissociation rates have previously been measured by dilution in the presence of a weaker, readily reversible, and competitive inhibitor which stabilizes the protein and allows for prolonged dissociation experiments (*21*). Previous reports with keto acid inhibitors of NS3 monitored dissociation over the course of a 60 h experiment (*21*). We attempted to similarly study ITMN-191 dissociation over an extended time. However, under the conditions of this study, the control sample lacking ITMN-191 lost significant activity within 16 h of the experiment, precluding any meaningful observations.

Additional evidence for the very slow dissociation of ITMN-191 was instead obtained by monitoring dissociation of the radiolabeled drug from WT NS3. An excess of unlabeled ITMN-191 was used to displace [^{14}C]ITMN-191 from a preformed NS3 complex, and the amount of [^{14}C]ITMN-191 released over time was monitored. Only 10% of drug dissociated from WT NS3 in 14 h, confirming the very slow dissociation of ITMN-191 (data not shown). Although the low level of dissociation precludes an accurate assessment, the dissociation rate constant is calculated to be

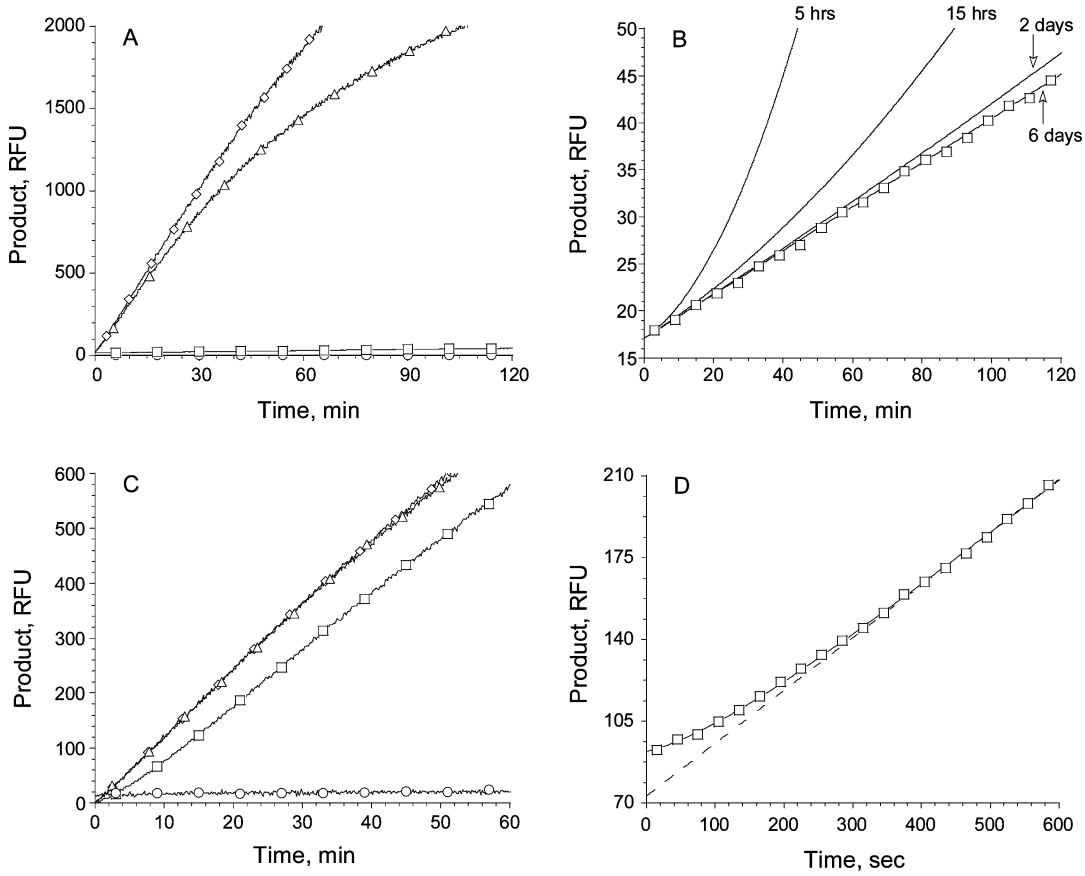

FIGURE 6: Reactivation of WT and R155K NS3 following dilution of their preformed ITMN-191 complexes. Panels A and C depict data for WT and R155K NS3, respectively. Progress curves collected following 10000-fold dilution to 0.1 nM NS3 and 0.2 nM ITMN-191 are shown (□) along with control reactions without either ITMN-191 (◇), NS3 (○), or enzyme−inhibitor preincubation (△). Panel B shows the extremely slow reactivation of WT NS3 (from panel A) on a reduced *y*-axis scale. Simulated progress curves assuming WT NS3·ITMN-191 complex half-lives of 5 h, 15 h, 2 days, and 6 days are shown. Panel D shows the reactivation of R155K NS3 (from panel C) on a reduced *x*-axis scale. The best fit using eq 1 and the steady-state rate (V_s) are shown as solid and dashed lines, respectively. The fit-derived reactivation rate constant is 9×10^{-3} s^{-1}.

$\sim 2.1 \times 10^{-6}$ s^{-1} ($t_{1/2} \sim 4$ days). In a similar experiment with D168A NS3, addition of excess unlabeled ITMN-191 resulted in immediate dissociation of [^{14}C]ITMN-191 (data not shown). These results are in agreement with dilution experiments that suggest the D168A substitution abrogates the slow dissociation of ITMN-191.

Simulation of the Kinetics of Binding of ITMN-191 to WT NS3. Progress curve data from NS3-initiated reactions (Figure 2) were globally fit to the proposed two-step binding mechanism (Materials and Methods). The following initial fit constraints were applied: $k_3 = 6.2 \times 10^{-2}$ s^{-1}, $k_4 = 3.8 \times 10^{-5}$ s^{-1}, $K_i = k_2/k_1 = 100$ nM, and $k_1 = 3.3 \times 10^4$ M^{-1} s^{-1}. The fit quality improved substantially when k_3, k_4, and K_i were fixed at the specified values while k_1 and k_2 were allowed to vary. The best fit k_1 and k_2 values are $\sim 3 \times 10^6$ M^{-1} s^{-1} and ~ 0.3 s^{-1}, respectively. These estimates complete the proposed mechanism for ITMN-191 binding (Figure 7).

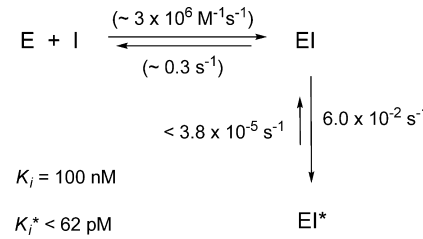

FIGURE 7: Kinetic summary of binding of ITMN-191 to WT NS3. Values for the rate and equilibrium constants associated with the proposed two-step binding mechanism are provided. Simulated rates are in parentheses.

DISCUSSION

Kinetic characterization of NS3 protease inhibition by ITMN-191 reveals slow and tight binding with an extremely slow dissociation that is unique among macrocyclic NS3 protease inhibitors. As slow dissociation allows persistent inhibition of NS3 protease activity and has potential clinical significance, the binding kinetics of ITMN-191 was characterized in detail. The results are consistent with a two-step binding mechanism in which an initial complex (EI) is rapidly formed and slowly converts to a more stable form (EI*). Microscopic rate constants within this mechanism were defined using a combination of enzyme inhibition assays and direct binding methods (Figure 7). Fitting biphasic reaction progress curves generated NS3 inactivation rate constants which show a hyperbolic dependence on ITMN-191 concentration. This dependence provides values for the affinity of the initial complex ($K_i = 100$ nM), the rate constant for the conversion of EI to EI* ($k_3 = 6.2 \times 10^{-2}$ s^{-1}), and the conversion of EI* to EI ($k_4 < 3.8 \times 10^{-5}$ s^{-1}). This k_4 estimate implies that the NS3·ITMN-191 complex has a half-life of ~ 5 h, if k_4 is assumed to be the rate-limiting step in dissociation. Protein fluorescence experiments independently verify the rate of isomerization of EI to EI* (k_3). Additional

experiments for directly determining the rate of ITMN-191 dissociation suggest the EI* complex may be considerably more stable. Surface plasmon resonance and dilution experiments provide estimates of ITMN-191 dissociation rate constants of $<2.1 \times 10^{-5}$ and $<1.3 \times 10^{-6}$ s^{-1} ($t_{1/2} > 9$ h and 6 days), respectively. However, the accuracy of these determinations is limited by the minimal dissociation or reactivation observed. Consequently, k_4 and K_i* are conservatively reported as $<3.8 \times 10^{-5}$ s^{-1} ($t_{1/2} > 5$ h) and <62 pM, respectively, as determined by indirect kinetic methods (Figure 7).

Slow dissociation from HCV NS3 protease has also been reported for the investigational drugs VX-950 and SCH-503034 that are currently in phase III clinical trials (*5, 6*). These inhibitors possess a keto amide functionality that reacts covalently and reversibly with the catalytic serine nucleophile S139 (*19, 20, 37, 38*). Their inhibition kinetics is consistent with an initial collision complex (EI) being formed that slowly converts to the more stable covalent complex (EI*). In the case of ITMN-191, however, the differences between EI and EI* states are not readily apparent.

Since $K_i = 100$ nM and $K_i^* < 62$ pM, the initial complex is strengthened at least 1600-fold upon isomerization to the EI* state. In free energy terms, this implies that the EI* state is stabilized by an additional 4.4 kcal/mol at 25 °C [calculated using the equation $\Delta G = -RT \ln(K_i^*/K_i)$, where R is the ideal gas constant and T is the temperature in kelvin]. Since the EI to EI* transition significantly changes protein fluorescence, some change in protein structure can be expected. Structures of NS3 in the presence and absence of bound ITMN-191 were compared to identify structural changes that may be involved in the conversion of EI to EI*. The key features of ITMN-191 binding and the binding of acyl sulfonamide inhibitors in general have been summarized elsewhere (*25, 39*−*42*). In the ITMN-191-bound state, the acyl sulfonamide group forms several polar contacts with residues in the oxyanion hole without formation of a covalent bond, while a network of polar interactions among residues R123, D168, and R155 helps define the P2 binding site. A comparison of ITMN-191-bound and apo NS3 structures reveals altered conformations of the three residues in this network of polar interactions as well as K136, suggesting their possible involvement in the slow transformation of EI to EI*.

Structure−activity relationships (SARs) between close ITMN-191 analogs indicate that it is unlikely that a single NS3 or ITMN-191 structural element is responsible for tight binding. An analog lacking P2 abrogates slow and tight binding (Figure 5), as do analogs that lack or modify the P1′ acyl-sulfonamide group, the P4 group, or the macrocyclic core (data not shown). These observations are consistent with the faster dissociation of TMC-435350 and BILN-2061 (*17, 43*), which lack P4 and P1′ groups, respectively. Thus, it is likely that an aggregate effect of optimized interactions between NS3 and ITMN-191 gives rise to its slow and tight binding behavior.

Preformed complexes of ITMN-191 and R155K NS3 or D168A NS3 are rapidly reactivated upon dilution, indicating that these amino acid substitutions compromise the slow dissociative property of ITMN-191. R155K and D168A disrupt the pattern of polar interactions that forms the P2 binding site (*25, 39*) and were identified as the major variants resistant to macrocyclic NS3 inhibitors in studies using the HCV replicon system (*25, 29, 30*). The loss of cellular potency promoted by these substitutions reflects an elevated inhibitor dissociation rate, a situation that is also seen with HIV-1 protease inhibitors. Indinavir, saquinavir, and other peptide-mimetic inhibitors dissociate slowly from the WT HIV-1 protease with half-lives of 10−100 min (*44*). The binding kinetics of clinically observed resistant mutants measured by surface plasmon resonance methods reveal elevated inhibitor off rates (*34, 45*). The second-generation drug darunavir which is indicated for use against multidrug resistant (MDR) HIV-1 partially restores the slow dissociative properties against the MDR mutants and improves cellular efficacy (*44*). Likewise with HCV NS3 inhibitors, the slow dissociative properties of current investigational drugs like VX-950, SCH-503034, and ITMN-191 are desirable features to maintain.

Many marketed drugs like celecoxib and finasteride dissociate very slowly from their targets. Slow dissociation of these drugs prevents the competition between substrate and inhibitor from reaching equilibrium. These drugs are thus said to operate under nonequilibrium conditions (*46*). Such slowly dissociating drugs occupy their target sites for extended times (defined as residence times) which may have clinical implications (*47*). A critical aspect of drugs with extended residence times is that they provide a longer duration of pharmacological effect than a similar compound that is in rapid equilibrium between bound and unbound states. For example, the pharmacological effect of finasteride (inhibition of dihydrotestosterone production) is observed for 72 h, which is significantly longer than the 24 h needed for the circulating drug to reach trough levels following a single oral dose (*48*). Because these slowly dissociating drugs promote persistent inhibition of their target enzymes, they can be dosed less frequently with a lower overall drug burden. The ability to use a smaller dose has the added benefit of reducing the potential for off-target inhibition and related toxicities.

In theory, an ideal dosing scheme for a slowly dissociating drug can be designed on the basis of its pharmacokinetics and the dissociative half-life of the drug−target complex. However, in practice, the aforementioned advantages of slow dissociating inhibitors are often mitigated by the pharmacodynamics of the drug target. Schramm and co-workers introduced the concept of "ultimate physiological inhibition" to describe a situation in which the pharmacologic effect of a drug is limited by the synthesis of new target protein. The authors demonstrate that a single oral dose of a very potent purine nucleotide phosphorylase (PNP) inhibitor in mice results in inhibition of circulating PNP activity that is only relieved by the synthesis of new PNP-containing erythrocytes (*49*). Other analogous examples include the inhibition of steroid 5α-reductase by finasteride (*48, 50*) and the inhibition of angiotensin II type 1 receptor (ATR1) by the antagonist candesartan (*51, 52*).

Assessing the true clinical impact of the slow dissociative property of drugs like ITMN-191, VX-950, and SCH-503034 is dependent on a reliable measure of viral protein turnover in infected human hepatocytes. To the best of our knowledge, a relevant measure of HCV protein synthesis has not been reported. The doubling time of HCV is ∼22 h in cell culture (*53*) and ∼6−8 h in infected patients and chimpanzees (*54, 55*).

If the time scale for viral protein turnover is similar, an appreciable contribution from slow dissociative behavior can be expected.

ACKNOWLEDGMENT

We thank Dr. Craig Cameron for helpful discussions and suggestions. We also thank Drs. Vladimir Serebryany and Leonid Beigelman for the synthesis of compounds used in the study.

SUPPORTING INFORMATION AVAILABLE

HCV NS3 protein sequences and progress curves for ITMN-191 inhibition of mutant NS3 proteases. This material is available free of charge via the Internet at http://pubs.acs.org.

REFERENCES

1. Shepard, C. W., Finelli, L., and Alter, M. J. (2005) Global epidemiology of hepatitis C virus infection. *Lancet Infect. Dis. 5*, 558–567.
2. National Institutes of Health (2002) NIH Consensus Statement on Management of Hepatitis C. NIH Consensus Statement, Vol. 19, pp 1−46, Bethesda, MD.
3. Fried, M. W., Shiffman, M. L., Reddy, K. R., Smith, C., Marinos, G., Goncales, F. L., Jr., Haussinger, D., Diago, M., Carosi, G., Dhumeaux, D., Craxi, A., Lin, A., Hoffman, J., and Yu, J. (2002) Peginterferon α-2a plus ribavirin for chronic hepatitis C virus infection. *N. Engl. J. Med. 347*, 975–982.
4. Manns, M. P., McHutchison, J. G., Gordon, S. C., Rustgi, V. K., Shiffman, M., Reindollar, R., Goodman, Z. D., Koury, K., Ling, M., and Albrecht, J. K. (2001) Peginterferon α-2b plus ribavirin compared with interferon α-2b plus ribavirin for initial treatment of chronic hepatitis C: A randomised trial. *Lancet 358*, 958–965.
5. Kwong, A. D., McNair, L., Jacobson, I., and George, S. (2008) Recent progress in the development of selected hepatitis C virus NS3.4A protease and NS5B polymerase inhibitors. *Curr. Opin. Pharmacol. 8*, 522–531.
6. Melnikova, I. (2008) Hepatitis C therapies. *Nat. Rev. Drug Discovery 7*, 799–800.
7. Yan, Y., Li, Y., Munshi, S., Sardana, V., Cole, J. L., Sardana, M., Steinkuehler, C., Tomei, L., De Francesco, R., Kuo, L. C., and Chen, Z. (1998) Complex of NS3 protease and NS4A peptide of BK strain hepatitis C virus: A 2.2 Å resolution structure in a hexagonal crystal form. *Protein Sci. 7*, 837–847.
8. Love, R. A., Parge, H. E., Wickersham, J. A., Hostomsky, Z., Habuka, N., Moomaw, E. W., Adachi, T., and Hostomska, Z. (1996) The crystal structure of hepatitis C virus NS3 proteinase reveals a trypsin-like fold and a structural zinc binding site. *Cell 87*, 331–342.
9. Kim, J. L., Morgenstern, K. A., Lin, C., Fox, T., Dwyer, M. D., Landro, J. A., Chambers, S. P., Markland, W., Lepre, C. A., O'Malley, E. T., Harbeson, S. L., Rice, C. M., Murcko, M. A., Caron, P. R., and Thomson, J. A. (1996) Crystal structure of the hepatitis C virus NS3 protease domain complexed with a synthetic NS4A cofactor peptide. *Cell 87*, 343–355.
10. Urbani, A., Biasiol, G., Brunetti, M., Volpari, C., Di Marco, S., Sollazzo, M., Orru, S., Piaz, F. D., Casbarra, A., Pucci, P., Nardi, C., Gallinari, P., De Francesco, R., and Steinkuhler, C. (1999) Multiple determinants influence complex formation of the hepatitis C virus NS3 protease domain with its NS4A cofactor peptide. *Biochemistry 38*, 5206–5215.
11. Bianchi, E., Urbani, A., Biasiol, G., Brunetti, M., Pessi, A., De Francesco, R., and Steinkuhler, C. (1997) Complex formation between the hepatitis C virus serine protease and a synthetic NS4A cofactor peptide. *Biochemistry 36*, 7890–7897.
12. Steinkuhler, C., Tomei, L., and De Francesco, R. (1996) In vitro activity of hepatitis C virus protease NS3 purified from recombinant baculovirus-infected Sf9 cells. *J. Biol. Chem. 271*, 6367–6373.
13. Johnson, C. L., Owen, D. M., and Gale, M., Jr. (2007) Functional and therapeutic analysis of hepatitis C virus NS3.4A protease control of antiviral immune defense. *J. Biol. Chem. 282*, 10792–10803.
14. Loo, Y. M., Owen, D. M., Li, K., Erickson, A. K., Johnson, C. L., Fish, P. M., Carney, D. S., Wang, T., Ishida, H., Yoneyama, M., Fujita, T., Saito, T., Lee, W. M., Hagedorn, C. H., Lau, D. T., Weinman, S. A., Lemon, S. M., and Gale, M., Jr. (2006) Viral and therapeutic control of IFN-β promoter stimulator 1 during hepatitis C virus infection. *Proc. Natl. Acad. Sci. U.S.A. 103*, 6001–6006.
15. Li, K., Foy, E., Ferreon, J. C., Nakamura, M., Ferreon, A. C., Ikeda, M., Ray, S. C., Gale, M., Jr., and Lemon, S. M. (2005) Immune evasion by hepatitis C virus NS3/4A protease-mediated cleavage of the Toll-like receptor 3 adaptor protein TRIF. *Proc. Natl. Acad. Sci. U.S.A. 102*, 2992–2997.
16. Foy, E., Li, K., Sumpter, R., Jr., Loo, Y. M., Johnson, C. L., Wang, C., Fish, P. M., Yoneyama, M., Fujita, T., Lemon, S. M., and Gale, M., Jr. (2005) Control of antiviral defenses through hepatitis C virus disruption of retinoic acid-inducible gene-I signaling. *Proc. Natl. Acad. Sci. U.S.A. 102*, 2986–2991.
17. Lamarre, D., Anderson, P. C., Bailey, M., Beaulieu, P., Bolger, G., Bonneau, P., Bos, M., Cameron, D. R., Cartier, M., Cordingley, M. G., Faucher, A. M., Goudreau, N., Kawai, S. H., Kukolj, G., Lagace, L., LaPlante, S. R., Narjes, H., Poupart, M. A., Rancourt, J., Sentjens, R. E., St George, R., Simoneau, B., Steinmann, G., Thibeault, D., Tsantrizos, Y. S., Weldon, S. M., Yong, C. L., and Llinas-Brunet, M. (2003) An NS3 protease inhibitor with antiviral effects in humans infected with hepatitis C virus. *Nature 426*, 186–189.
18. Reiser, M., Hinrichsen, H., Benhamou, Y., Reesink, H. W., Wedemeyer, H., Avendano, C., Riba, N., Yong, C. L., Nehmiz, G., and Steinmann, G. G. (2005) Antiviral efficacy of NS3-serine protease inhibitor BILN-2061 in patients with chronic genotype 2 and 3 hepatitis C. *Hepatology 41*, 832–835.
19. Perni, R. B., Almquist, S. J., Byrn, R. A., Chandorkar, G., Chaturvedi, P. R., Courtney, L. F., Decker, C. J., Dinehart, K., Gates, C. A., Harbeson, S. L., Heiser, A., Kalkeri, G., Kolaczkowski, E., Lin, K., Luong, Y. P., Rao, B. G., Taylor, W. P., Thomson, J. A., Tung, R. D., Wei, Y., Kwong, A. D., and Lin, C. (2006) Preclinical profile of VX-950, a potent, selective, and orally bioavailable inhibitor of hepatitis C virus NS3-4A serine protease. *Antimicrob. Agents Chemother. 50*, 899–909.
20. Lin, C., Kwong, A. D., and Perni, R. B. (2006) Discovery and development of VX-950, a novel, covalent, and reversible inhibitor of hepatitis C virus NS3.4A serine protease. *Infect. Disord.: Drug Targets 6*, 3–16.
21. Narjes, F., Brunetti, M., Colarusso, S., Gerlach, B., Koch, U., Biasiol, G., Fattori, D., De Francesco, R., Matassa, V. G., and Steinkuhler, C. (2000) α-Ketoacids are potent slow binding inhibitors of the hepatitis C virus NS3 protease. *Biochemistry 39*, 1849–1861.
22. Bradford, W. Z., Rubino, C., Porter, S., Forrest, A., Blatt, L. M., and Patat, A. A. (2008) A phase 1 study of the safety, tolerability, and pharmacokinetics of single ascending oral doses of the NS3/4A protease inhibitor ITMN-191 in healthy subjects. *Hepatology 48* (S1), 1146A.
23. Forestier, N., Larrey, D. G., Guyader, D., Marcellin, P., Rouzier, R., Patat, A. A., Bradford, W. Z., Porter, S., and Zeuzem, S. (2008) Treatment of Chronic Hepatitis C Virus (HCV) Genotype 1 Patients with the NS3/4A Protease Inhibitor ITMN-191 Leads to Rapid Reductions in Plasma HCV RNA: Results of a Phase 1b Multiple Ascending Dose (MAD) Study. *Hepatology 48* (S1), 1132A.
24. Rubino, C., Bradford, W. Z., Forrest, A., Porter, S., Blatt, L. M., Seiwert, S. D., and Zeuzem, S. (2008) Pharmacokinetic-Pharmacodynamic (PK-PD) Relationships for ITMN-191 in a Phase 1 Multiple Ascending Dose Trial in Patients with Genotype 1 Chronic Hepatitis C Infection. *Hepatology 48* (S1), 1140A–1141A.
25. Seiwert, S. D., Andrews, S. W., Jiang, Y., Serebryany, V., Tan, H., Kossen, K., Rajagopalan, P. T., Misialek, S., Stevens, S. K., Stoycheva, A., Hong, J., Lim, S. R., Qin, X., Rieger, R., Condroski, K. R., Zhang, H., Do, M. G., Lemieux, C., Hingorani, G. P., Hartley, D. P., Josey, J. A., Pan, L., Beigelman, L., and Blatt, L. M. (2008) Preclinical characteristics of the HCV NS3/4A protease inhibitor ITMN-191 (R7227). *Antimicrob. Agents Chemother. 52*, 4432–4441.
26. Sumpter, R., Jr., Wang, C., Foy, E., Loo, Y. M., and Gale, M., Jr. (2004) Viral evolution and interferon resistance of hepatitis C virus RNA replication in a cell culture model. *J. Virol. 78*, 11591–11604.
27. Sali, D. L., Ingram, R., Wendel, M., Gupta, D., McNemar, C., Tsarbopoulos, A., Chen, J. W., Hong, Z., Chase, R., Risano, C., Zhang, R., Yao, N., Kwong, A. D., Ramanathan, L., Le, H. V., and Weber, P. C. (1998) Serine protease of hepatitis C virus

expressed in insect cells as the NS3/4A complex. *Biochemistry 37*, 3392–3401.
28. Mao, S. S., DiMuzio, J., McHale, C., Burlein, C., Olsen, D., and Carroll, S. S. (2008) A time-resolved, internally quenched fluorescence assay to characterize inhibition of hepatitis C virus nonstructural protein 3-4A protease at low enzyme concentrations. *Anal. Biochem. 373*, 1–8.
29. He, Y., King, M. S., Kempf, D. J., Lu, L., Lim, H. B., Krishnan, P., Kati, W., Middleton, T., and Molla, A. (2008) Relative replication capacity and selective advantage profiles of protease inhibitor-resistant hepatitis C virus (HCV) NS3 protease mutants in the HCV genotype 1b replicon system. *Antimicrob. Agents Chemother. 52*, 1101–1110.
30. Seiwert, S. D., Hong, J., Lim, S. R., Tan, H., Kossen, K., and Blatt, L. M. (2006) Sequence variation of NS3 and NS4A in hepatitis C virus (HCV) replicons following exposure to ITMN-191 concentrations likely to encompass those achieved in human liver following clinical dosing. First international workshop on hepatitis C resistance & new compounds, October 25−26, Boston, MA.
31. Bull, H. G., Thornberry, N. A., Cordes, M. H., Patchett, A. A., and Cordes, E. H. (1985) Inhibition of rabbit lung angiotensin-converting enzyme by Nα-[(S)-1-carboxy-3-phenylpropyl]-L-alanyl-L-proline and Nα-[(S)-1-carboxy-3-phenylpropyl]-L-lysyl-L-proline. *J. Biol. Chem. 260*, 2952–2962.
32. Gould, W. R., Cladera, E., Harris, M. S., Zhang, E., Narasimhan, L., Thorn, J. M., and Leadley, R. J., Jr. (2005) Co-crystal structure and inhibition of factor Xa by PD0313052 identifies structurally stabilized active site residues of factor Xa and prothrombinase. *Biochemistry 44*, 9280–9289.
33. Furfine, E. S., D'Souza, E., Ingold, K. J., Leban, J. J., Spector, T., and Porter, D. J. (1992) Two-step binding mechanism for HIV protease inhibitors. *Biochemistry 31*, 7886–7891.
34. Maschera, B., Darby, G., Palu, G., Wright, L. L., Tisdale, M., Myers, R., Blair, E. D., and Furfine, E. S. (1996) Human immunodeficiency virus. Mutations in the viral protease that confer resistance to saquinavir increase the dissociation rate constant of the protease-saquinavir complex. *J. Biol. Chem. 271*, 33231–33235.
35. Copeland, R. A. (2005) *Evaluation of enzyme inhibitors in drug discovery. A guide for medicinal chemists and pharmacologists*, pp 141−213, Wiley-Interscience, New York.
36. Van Aller, G. S., Nandigama, R., Petit, C. M., DeWolf, W. E., Jr., Quinn, C. J., Aubart, K. M., Zalacain, M., Christensen, S. B., Copeland, R. A., and Lai, Z. (2005) Mechanism of time-dependent inhibition of polypeptide deformylase by actinonin. *Biochemistry 44*, 253–260.
37. Malcolm, B. A., Liu, R., Lahser, F., Agrawal, S., Belanger, B., Butkiewicz, N., Chase, R., Gheyas, F., Hart, A., Hesk, D., Ingravallo, P., Jiang, C., Kong, R., Lu, J., Pichardo, J., Prongay, A., Skelton, A., Tong, X., Venkatraman, S., Xia, E., Girijavallabhan, V., and Njoroge, F. G. (2006) SCH 503034, a mechanism-based inhibitor of hepatitis C virus NS3 protease, suppresses polyprotein maturation and enhances the antiviral activity of α interferon in replicon cells. *Antimicrob. Agents Chemother. 50*, 1013–1020.
38. Njoroge, F. G., Chen, K. X., Shih, N. Y., and Piwinski, J. J. (2008) Challenges in modern drug discovery: A case study of boceprevir, an HCV protease inhibitor for the treatment of hepatitis C virus infection. *Acc. Chem. Res. 41*, 50–59.
39. Condroski, K. R., Zhang, H., Ballard, J. A., Bernat, B. A., Brandhuber, B. J., Andrews, S. W., Josey, J. A., and Blatt, L. M. (2006) Structure-based design of novel isoindoline inhibitors of HCV NS3/4A protease and binding mode analysis of ITMN-191 by X-ray crystallography. *Gastroenterology 130* (4, Suppl. 2), A835.
40. Poliakov, A., Johansson, A., Akerblom, E., Oscarsson, K., Samuelsson, B., Hallberg, A., and Danielson, U. H. (2004) Structure-activity relationships for the selectivity of hepatitis C virus NS3 protease inhibitors. *Biochim. Biophys. Acta 1672*, 51–59.
41. Ronn, R., Gossas, T., Sabnis, Y. A., Daoud, H., Kerblom, E., Danielson, U. H., and Sandstrom, A. (2007) Evaluation of a diverse set of potential P1 carboxylic acid bioisosteres in hepatitis C virus NS3 protease inhibitors. *Bioorg. Med. Chem. 15*, 4057–4068.
42. Ronn, R., Sabnis, Y. A., Gossas, T., Akerblom, E., Danielson, U. H., Hallberg, A., and Johansson, A. (2006) Exploration of acyl sulfonamides as carboxylic acid replacements in protease inhibitors of the hepatitis C virus full-length NS3. *Bioorg. Med. Chem. 14*, 544–559.
43. Lin, T., Devogelaere, B., Lenz, O., Nyanguile, O., van der Helm, E., Vermeiren, K., Vandercruyssen, G., Cleiren, E., Lindberg, J., Edlund, M., Raboisson, P., de Kock, H., Cummings, M., Fanning, G., and Simmen, K. (2008) Inhibitory activity of TMC435350 on HCV NS3/4A proteases from genotypes 1 to 6. *Hepatology 48* (S1), 1166A.
44. Dierynck, I., De Wit, M., Gustin, E., Keuleers, I., Vandersmissen, J., Hallenberger, S., and Hertogs, K. (2007) Binding kinetics of darunavir to human immunodeficiency virus type 1 protease explain the potent antiviral activity and high genetic barrier. *J. Virol. 81*, 13845–13851.
45. Shuman, C. F., Markgren, P. O., Hamalainen, M., and Danielson, U. H. (2003) Elucidation of HIV-1 protease resistance by characterization of interaction kinetics between inhibitors and enzyme variants. *Antiviral Res. 58*, 235–242.
46. Swinney, D. C. (2004) Biochemical mechanisms of drug action: What does it take for success? *Nat. Rev. Drug Discovery 3*, 801–808.
47. Copeland, R. A., Pompliano, D. L., and Meek, T. D. (2006) Drug-target residence time and its implications for lead optimization. *Nat. Rev. Drug Discovery 5*, 730–739.
48. Tian, G. (1996) In vivo time-dependent inhibition of human steroid 5 α-reductase by finasteride. *J. Pharm. Sci. 85*, 106–111.
49. Lewandowicz, A., Tyler, P. C., Evans, G. B., Furneaux, R. H., and Schramm, V. L. (2003) Achieving the ultimate physiological goal in transition state analogue inhibitors for purine nucleoside phosphorylase. *J. Biol. Chem. 278*, 31465–31468.
50. Bull, H. G., Garcia-Calvo, M., Andersson, S., Baginsky, W. F., Chan, H. K., Ellsworth, D. E., Miller, R. R., Stearns, R. A., Bakshi, R. K., Rasmusson, G. H., Tolman, R. L., Myers, R. W., Kozarich, J. W., and Harris, G. S. (1996) Mechanism-Based Inhibition of Human Steroid 5a-Reductase by Finasteride: Enzyme-Catalyzed Formation of NADP-Dihydrofinasteride, a Potent Bisubstrate Analog Inhibitor. *J. Am. Chem. Soc. 118*, 2359–2365.
51. Vanderheyden, P. M., Fierens, F. L., and Vauquelin, G. (2000) Angiotensin II type 1 receptor antagonists. Why do some of them produce insurmountable inhibition? *Biochem. Pharmacol. 60*, 1557–1563.
52. Lacourciere, Y., and Asmar, R. (1999) A comparison of the efficacy and duration of action of candesartan cilexetil and losartan as assessed by clinic and ambulatory blood pressure after a missed dose, in truly hypertensive patients: A placebo-controlled, forced titration study. Candesartan/Losartan study investigators. *Am. J. Hypertens. 12*, 1181–1187.
53. Zhong, J., Gastaminza, P., Cheng, G., Kapadia, S., Kato, T., Burton, D. R., Wieland, S. F., Uprichard, S. L., Wakita, T., and Chisari, F. V. (2005) Robust hepatitis C virus infection in vitro. *Proc. Natl. Acad. Sci. U.S.A. 102*, 9294–9299.
54. Tanaka, J., Katayama, K., Kumagai, J., Komiya, Y., Yugi, H., Kishimoto, S., Mizui, M., Tomoguri, T., Miyakawa, Y., and Yoshizawa, H. (2005) Early dynamics of hepatitis C virus in the circulation of chimpanzees with experimental infection. *Intervirology 48*, 120–123.
55. Neumann, A. U., Lam, N. P., Dahari, H., Gretch, D. R., Wiley, T. E., Layden, T. J., and Perelson, A. S. (1998) Hepatitis C viral dynamics in vivo and the antiviral efficacy of interferon-α therapy. *Science 282*, 103–107.

BI900038P